Supporting Information

Renaud et al. 10.1073/pnas.1309139110

SI Text

Stochastic Surrogate Hamiltonian Model for Short DNA Hairpins

Following the stochastic surrogate Hamiltonian (SSH) approach, the simulation of the charge transfer is performed solving the Liouville equation for the full density matrix, $\rho(t)$:

$$\frac{d\rho(t)}{dt}=\frac{-i}{\hbar}[\mathcal{H}_S+\mathcal{H}_B+\mathcal{H}_{SB};\rho(t)], \qquad [S1]$$

where $\mathcal{H}_S$ is the Hamiltonian modeling the hairpin, $\mathcal{H}_B$ is the Hamiltonian of the bath formed by the intramolecular vibration modes of the individual molecule in the hairpin, and $\mathcal{H}_{SB}$ is the interaction Hamiltonian between the propagating hole and the bath. Following our previous study (1), the Hamiltonian of the system reads:

$$\begin{aligned}\mathcal{H}_S=&E_{S_a}|S_a\rangle\langle S_a|+\sum_{i=1}^{N}E_i|B_i\rangle\langle B_i|+E_{S_b^*}|S_b^*\rangle\langle S_b^*|\\&+\sum_{i=1}^{N}(E_i-E_t)|t_i\rangle\langle t_i|+E_{S_b}|S_b\rangle\langle S_b|\\&+c_a|S_a\rangle\langle B_1|+c_b|B_N\rangle\langle S_b^*|\\&+\sum_{i=1}^{N-1}\alpha_{i,i+1}|B_i\rangle\langle B_{(i+1)}|\\&+h.c..\end{aligned} \qquad [S2]$$

In this Hamiltonian, E_{S_a} is the energy of the excited state, $|S_a\rangle$, of the hole donor. Similarly, $E_{S_b^*}$ is the on-site energy of the excited state, $|S_b^*\rangle$, of the hole acceptor. The values of these two energies is set as the reference (i.e., $E_{S_a}=E_{S_b^*}=0$). In our model, E_i is the on-site energy of the state $|B_i\rangle$ representing the ith base pair in the hairpin. The value of this energy is defined following a Weller-like equation:

$$E_n=\mathrm{IP}_{B_n}-E_{h\nu}-\mathrm{EA}_{S_a}+E_c\left(S_a^-/B_n^+\right)-\Delta E_{\mathrm{solv}}, \qquad [S3]$$

where IP_{B_n} is the ionization potential (IP) of the nth base pair, $\mathrm{EA}_{S_a}=1.08$ eV is the electron affinity of the hole donor (2), and $E_{h\nu}=3.35$ eV is the excitation energy of the stilbene donor (3). $E_c(S_a^-/B_n^+)$ is the Coulomb attraction between the electron excess located on S_a and the propagating hole, and $\Delta E_{\mathrm{solv}}=0.2$ eV is the solvation energy (2). The only difference between an A:T base pair and a G:C base pair in our model is therefore the IP of the corresponding site. It is commonly accepted that the IP of the guanine molecule is ∼0.5 eV lower than the IP of the adenine molecule (4, 5), which partially explains the high conductance of hairpin presenting a high concentration of G:C base pairs. Hence the IP of adenine and guanine are respectively fixed to $\mathrm{IP}_A=7.35$ eV and $\mathrm{IP}_G=6.86$ eV. Finally, the energy, E_{S_b}, of the ground state of the anionic form of the hole acceptor, $|S_b\rangle$, is set to –0.25 eV (1).

The states mentioned above are all coupled with each other to enable the hole to transfer from one base pair to another. All these couplings have been evaluated via density functional theory calculations by Grozema et al. (2, 6). The coupling c_a between the hole donor and the first base pair is equal to 5(−4) meV if the first base pair is A:T(G:C). Similarly, the coupling between the last base pair and the hole acceptor is set to 25(80) meV if the last base pair is A:T(G:C). Finally, the coupling $\alpha_{i,i+1}$ is set to 50 meV between two A:T base pairs and to −4 meV between an A:T base pair and a G:C base pair.

The geometry relaxation of individual base pairs upon charging tends to localize the propagating hole. To simulate such localization, trap states, labeled $|t_i\rangle$, are introduced in our model. The intramolecular energy relaxation, labeled E_t, was estimated by comparing the vertical and adiabatic IP of the base pairs, leading to a value of ∼0.15 eV (1).

In the SSH approach, the bath is defined as series of two-level systems, or quantum modes, and its Hamiltonian reads:

$$\mathcal{H}_B=\sum_{i=1}^{M}\hbar\omega_i\boldsymbol{\sigma}_i^{\dagger}\boldsymbol{\sigma}_i, \qquad [S4]$$

where ω_i is the frequency of the ith mode and $\boldsymbol{\sigma}_i^{\dagger}(\boldsymbol{\sigma}_i)$ is the creation (annihilation) operator. The value of the mode frequencies, ω_i, was chosen to fit the intramolecular vibrations modes of the isolated base pairs using a super-ohmic distribution (7, 8):

$$\mathcal{J}(\omega)=\lambda(\omega/\omega_c)^2e^{-(\omega/\omega_c)^2}, \qquad [S5]$$

with the cutoff frequency, ω_c, set at $\omega_c=0.15$ eV. The reorganization energy, λ, was set to $\lambda=100$ meV, which is a typical value of hole–phonon interaction strength in the adenine and guanine molecules (9). Finally, the interaction Hamiltonian between the propagating hole on the hairpin and the bath formed by intramolecular vibration modes is given by:

$$\mathcal{H}_{SB}=\mathcal{R}_S\otimes\sum_{i=1}^{M}\frac{\mathcal{J}(\omega_i)}{\sqrt{M}}\left(\boldsymbol{\sigma}_i^{\dagger}+\boldsymbol{\sigma}_i\right), \qquad [S6]$$

where $\mathcal{R}_S$ is the dimensionless relaxation pathway matrix and $\mathcal{J}(\omega_i)$ is the spectral density of the hole-phonon coupling constant (unit of energy), evaluated at the bath-mode frequency ω_i. The $1/\sqrt{M}$ term was introduced for our simulation to converge when increasing the number of bath modes, M, explicitly incorporated in our calculations. The relaxation matrix accounts for the trapping on the base pairs as well as the final trapping on hole acceptor, and consequently reads:

$$\mathcal{R}_S=\left(|S_b^*\rangle\langle S_b|+\sum_{i=1}^{N}|B_i\rangle\langle t_i|+h.c.\right). \qquad [S7]$$

The initial state of the evolution was set as a product state: $\rho(0)=\rho_S(0)\otimes\rho_B(T)$, where $\rho_S(0)=|S_a\rangle\langle S_a|$ and $\rho_B(T)$ represent the thermal state of the bath. This initial state can lead to nonphysical results when accounting explicitly for the excitation pulse because it ignores the inherent system/bath entanglement. However, it is acceptable in our case because the evolution directly starts from the excited state of the hole donor (i.e., after the excitation pulse, where the initial system/bath entanglement has been partially or totally destroyed). To limit the computational cost of the approach, only a small number of bath modes are explicitly incorporated in $\mathcal{H}_B$. To delay the recurrence time, the SSH approach uses quantum jumps in the bath manifold. Each of these jumps resets the state of a given bath mode to its thermal state, and consequently simulates the exchange of energy between the explicit bath and a larger unresolved environment.

Further details about the implementation of the SSH approach can be found in the study by Renaud et al. (1).

Hole Dynamics

Hole Migration Along *GA*. Fig. S1*A* presents the evolution of the charge density along *GA*. Starting from the hole donor, the hole density is quickly transferred to the neighboring G:C base pair, where almost 80% of the hole density is localized after 2 ps. This important localization of the hole density on the first base pair was also observed in poly(A)-poly(T) hairpins (1). This initial localization on the first base pair of the sequence is here reinforced by the low IP of the G:C base pair. Despite this important initial localization, the hole density slowly propagates onto the neighboring A:T base pair, from which it can finally reach the hole acceptor. However, due to the important localization on the G:C base pair, the transfer rate to S_b is inefficient; only less than 10% of the hole density has reached the acceptor after 25 ps, and only less than 20% has reached the acceptor after 100 ps (Fig. S3*A*).

Hole Migration Along *AG*. Fig. S1*B* presents the hole propagation along hairpin *AG*. These dynamics present radically different characteristics than the one obtained along *GA*. Initially localized on S_a, the hole density is rapidly transferred onto the neighboring A:T base pair. However, a maximum of only 50% of the hole density is localized on this base pair after 1 ps against 80% for hairpin *GA*. This weaker localization is mainly due to the rapid transfer that occurs between the two base pairs allowed by their small energy difference. When the G:C is located after the A:T base pair, the difference in their IP compensates for the Coulomb energy term in Eq. **S3**. This gives an energy difference of only 0.3 eV between the two base pairs. With such a small energy gap to overcome, the charge is quickly transferred to the second base pair, where almost 40% of the hole density is localized after 2 ps. Due to its low IP, the energy difference between the G:C base pair located at the end of the hairpin and the hole acceptor is also reduced compared with the previous case, which speeds up the last transfer step. As a result, the overall transfer is much more efficient than in hairpin *GA*, and more than 50% of the hole density has already crossed the hairpin and reaches the hole acceptor after 25 ps. As seen in Fig. S3*A*, the hole density localized on S_b saturates to 61% after about 100 ps.

Hole Dynamics Along GA_5. Fig. S2*A* presents the hole dynamics along hairpin GA_5, together with the site energies of the base pairs along this sequence. The hole is initially localized on the donor site S_a and is transferred to the neighboring G base, where almost 75% of the hole population is localized after 2 ps. As seen in Fig. S2*A*, the energy difference between the first and second base pairs is equal to 1.3 eV. This large energy difference significantly slows down the process of hole migration such that more than 50% of the hole population is still localized on the first G:C base pair after 10 ps. Hence, the G:C base pair in the GA_5 sequence can be considered as an efficient trap for the hole density. Nevertheless, there exists a certain probability that a hole will escape localization on the G:C site and will slowly propagate along the hairpin. However, after 25 ps, only 10% of the hole density has reached the last base pair and less than 0.1% of the hole density is localized on the hole acceptor (Fig. S3*B*). Even after 100 ps, only 1% of the hole density is localized on S_b.

Hole Dynamics Along A_5G. Fig. S2*B* presents the hole dynamics involved in hairpin A_5G, together with the site energies of the base pairs along this sequence. Similar to the GA_5 hairpin, the hole undergoes a fast transfer from S_a to the first A:T base pair. The site energy of this base pair is 0.5 eV larger than that of the G:C pair in GA_5 (compare with energy diagrams in Fig. S2 *A* and *B*). For this reason, the hole localization on the first base pair is less effective for A_5G than for GA_5. As a result, in the case of the A_5G sequence, only 60% of the hole population is localized on the first A:T base pair after 2 ps. It is worth mentioning that the energy difference between the first two base pairs is smaller for A_5G (0.8 eV) than for GA_5 (1.3 eV). This allows a faster hole transfer from the first base pair to the rest of the hairpin. Therefore, after 25 ps, 20% of the charge population has reached the last G:C base pair and 0.25% of the hole density is localized on the hole acceptor (Fig. S3*B*). Even after 100 ps, only 2.5% of the hole density is localized on S_b.

Determination of k_a and Φ_a

The values of the charge separation quantum yield (Φ_a) and arrival rate (k_a) can be obtained by fitting the population of the hole acceptor site by the function:

$$\mathrm{Tr}[\rho(t)P_{S_b}] = \Phi_a\left(1 - e^{-(k_a t)^{\chi}}\right), \qquad \textbf{[S8]}$$

where $P_{S_b} = |S_b^*\rangle\langle S_b^*| + |S_b\rangle\langle S_b|$ is the projector on the S_b site. The values of k_a, Φ_a, and χ deduced from this fitting procedure for all the sequences studied in this article are listed in Table S1. The values of k_a and Φ_a obtained for hairpins A_2GA_3 and A_3GA_2 were the same, and only the latter are reported in Table S1. A stretched exponential parameter, $\chi = 1.1 - 1.3$, was necessary to obtain a satisfying fit for hairpins containing three to six base pairs. In such systems, the hole density is first transferred from S_a to the base pair stack before reaching the hole acceptor. Such sequential transfer induces a delay in the rise of the S_b population. This stretched exponential behavior is clearly visible in Fig. S3*B*. Note that our data only cover times up to 100 ps. As seen in Fig. S3*B*, this evolution time is not long enough to reach saturation of the S_b population for most hairpins. Hence, the fidelity of our fits may deteriorate for longer times. A stretched exponential, $\chi < 1$, was also necessary for short hairpins containing one to two base pairs. This deviation from the simple exponential is due to the competition between direct superexchange from S_a to S_b and sequential hopping via the base pairs. Consequently, fitting our data with a biexponential rise may be more suitable.

Fit of the Arrival Rate Distance Dependence

The variation of k_a with the distance, R, between S_a and S_b obtained for the different series represented in Fig. 1 can all be fitted by the equation:

$$k_a(R) = \kappa_1 e^{-\beta(N+1)R_0} + \kappa_2(N+1)^{-\eta}, \qquad \textbf{[S9]}$$

The first term of Eq. **S9** corresponds to a superexchange mechanism that gives rise to an exponential decay of the arrival rate with a falloff parameter β. The second term corresponds to the incoherent regime characterized by a power law of exponent η. Finally, κ_1 and κ_2 are the scaling factors of these two mechanisms. The values of these parameters obtained for our calculations are shown in Table S2. As seen in this table, β is sensitive to the sequence of the hairpin and goes from 0.85 Å^{-1} for the A_n series to 0.55 Å^{-1} for the A_nG series. This decrease of β is due to the lower energy barrier the hole has to overcome to cross hairpins containing a G:C base pair thanks to the low IP of G bases. The value of η is insensitive to the sequence and remains around $\eta = 2$. This value is typical of unbiased incoherent hopping. The value of κ_1 is also insensitive to the sequence. On the contrary, κ_2 varies significantly with the composition of the hairpins and goes from 1.6 ns^{-1} for the A_n series to 20 ns^{-1} for the A_nG series.

Degree of Delocalization and Participation Ratio

The hole transfer mechanism along sequences containing a single G:C base pair is usually described in terms of two sequential hopping steps: the first one from the hole donor to the G:C base pair and the second one from the G:C base pair to the hole acceptor

(10). This argument supposes a very weak population of the A:T base pairs during the transport, which implies a superexchange type of mechanism for this two elementary hopping steps.

To verify if our results match this sequential tunneling model, one can compute the degree of localization of the hole density following:

$$\mathcal{L} = \frac{1}{T}\int_0^T \sum_n \left(Tr\left[\rho(t)P_n\right]\right)^2 dt, \qquad \textbf{[S10]}$$

where P_n is the projector on the nth site and the index n runs over the hole donor, the different base pairs, and the hole acceptor. If the hole is completely localized on a given base pair at time t, the quantity $\sum_n (Tr[\rho(t)P_n])^2$ equals 1 and falls down to $1/N$ when the hole is delocalized over N different sites. In Eq. **S10,** $\mathcal{L}$ depends on the time-averaging value T. We pose here $T = 5$ ps so that $\mathcal{L}$ will not be dominated by the slow propagation of the hole density from the base pair to the hole acceptor. The corresponding values are reported in Table S3 for different sequences containing six base pairs each. These values remains quite low for all sequences, indicating a strong delocalization of the hole density along the hairpin. This important delocalization is illustrated in Fig. 3. To grasp the impact of guanine on the hole propagation, one can compute the change in $\mathcal{L}$, noted as $\Delta\mathcal{L}$, induced by the introduction of a G:C base pair at a given site. These values, reported in Table S3, show that substituting the first A:T with a G:C base pair increases the degree of localization by 39%. This increase of $\mathcal{L}$ is due to the efficient trapping of the hole density on the G:C base pair seen in Fig. S1*A*. On the contrary, performing the A:T/G:C substitution at the second site decreases $\mathcal{L}$ by 13%. This decrease of $\mathcal{L}$ here is due to the rapid charge transfer between the first and second base pairs that occurs in that case, as seen in Fig. S1*B*. However, introducing a G:C base pair in third position or further away from S_a does not significantly modify the degree of localization.

The degree of localization of the hole density on the G:C base pair can be also evaluated from the participation ratio of the G:C base pair given by:

$$\mathcal{R}_G = \frac{1}{T}\int_0^T \frac{Tr\left[\rho(t)P_G\right]}{\sum_n Tr\left[\rho(t)P_n\right]}, \qquad \textbf{[S11]}$$

where P_G is the projector on the G:C base pair and the index n runs over all the base pairs S_a and S_b, and $T = 5$ ps (see previous section). The corresponding values of $\mathcal{R}_G$ are reported in Table S3 for different sequences containing six base pairs. The larger participation ratio is obtained when the G:C base pair is in first position due to the strong localization of the hole density observed in that case. Shifting the position of the G:C base pair toward the end of the sequence decreases $\mathcal{R}_G$. One can also compare the values of $\mathcal{R}_G$ with the participation ratio of an A:T base pair at the same position in hairpin A_6. The corresponding values, noted $\Delta\mathcal{R}_G$, are reported in Table S3. The larger modification is obtained when the G:C base pair is in the second position. In A_6, the transfer from S_a to the first base pair is fast but the subsequent transfer from the first base pair to the second base pair is much slower due to the large energy difference between these two sites. In AGA_4, a small energy difference is obtained between the first A:T base pair and the G:C base pair, which leads to a rapid transfer from S_a to the these two base pairs.

Our results show that according to our simulations, the G:C base pair does not act as an intermediary residing site where the hole density localizes during its propagation. Much like in the case of poly(A)-poly(T) sequences (1), the hole density is delocalized along the entire hairpin and only partially occupies the G:C base pair. The participation ratio of the G:C base pair depends on its position along the hairpin and, of course, the length of the sequence. However, the G:C base pair is never fully populated. As mentioned in the main text, our model ignores the solvent reorganization that could induce a strong localization of the propagating charge.

Nearest Neighbor Transfer Rates

The computation of the nearest neighbor transfer rate, $k_{n,n+1}$, between the nth and $(n+1)$th base pairs relies on the evaluation of the transfer rates, k_n and k_{n+1}, from S_a to each of these sites (1). The values of k_n and k_{n+1} can be obtained by fitting the temporal evolution of the hole population on the nth and $(n+1)$th sites with a rising exponential function (1). Once these two kinetic parameters are evaluated, the transfer rate $k_{n,n+1}$ is computed following the method of Renaud et al. (1):

$$k_{n,n+1} = \frac{k_n k_{n+1}}{k_n - k_{n+1}}. \qquad \textbf{[S12]}$$

Note that the final transfer rate, k_f, from the last base pair to the acceptor S_b can also be computed following Eq. **S12**. However, in this case, k_{n+1} should be replaced by the arrival rate k_a. The values of the nearest neighbor transfer rates calculated for hairpin A_6 and for three different sequences containing a single G:C are reported in Table S4. The results listed in this table show that the nearest neighbor transfer rates obtained for A_6 continuously increase along the hairpin due to the progressive reduction of the energy difference between neighboring pairs (1). In addition, the large energy difference between the last A:T pair and the hole acceptor leads to a value of k_f that is three orders of magnitude smaller than the average rate of hole transfer between neighboring base pairs. Therefore, this last transfer step is the limiting step of the entire hole propagation along hairpin A_6. Examination of Table S4 reveals that this conclusion is also valid for the other sequences studied in this article. Note that k_f is one order of magnitude larger for A_5G than for A_6. This significant increase of the final transfer rate can be attributed to the low IP of the guanine base. A lower IP leads to a smaller energy difference between the last base and the hole acceptor in A_5G than in A_6, thus increasing the transfer rate. For this reason, difference in k_a values obtained for hairpins A_5G and A_6 can mainly be attributed to changes in the rate of the last transfer step only.

As can be seen from Table S4, the forward hole transfer rate from a G:C base pair to its neighboring A:T base pair at a given position along the sequence is always slower than the transfer rate at the same position in A_6 (values marked in red in Table S4). On the contrary, the forward transfer rate from an A:T base pair to the following G:C base pair can be either larger or smaller than the transfer rate at the same position in A_6 (values marked in blue in Table S4). To understand this result, it is useful to recognize that due to the electrostatic interaction between the moving hole and S_a^-, the energy of the nth site is smaller than the energy of the $(n+1)$th site. Substituting the nth A:T base pair for a G:C base pair increases this energy difference, and consequently reduces the transfer rate $k_{n,n+1}$. Another situation arises when replacing the $(n+1)$th A:T base pair with a G:C base pair. This substitution can either decrease or increase the energy difference between the two neighboring base pairs depending on their location in the sequence. This, in turn, will make the value of the rate for hole transfer between these adjacent pairs either greater or smaller.

Delocalized Conduction Channels

As mentioned in the main text, the delocalized conduction channels (DCCs) appear after a bloc-diagonalization of the hairpins Hamiltonian. Ignoring the dynamical disorder, the static Hamiltonian describing the hole propagation on the hairpin reads:

$$\mathcal{H} = \begin{pmatrix} E_{S_A} & c_a & & & & \\ c_a & E_1 & \alpha_1 & & & \\ & \alpha_1 & \ddots & \ddots & & \\ & & \ddots & \ddots & \alpha_N & \\ & & & \alpha_N & E_N & c_b \\ & & & & c_b & E_{S_b} \end{pmatrix}. \quad \textbf{[S13]}$$

The diagonalization of the Hamiltonian on the subspace spanned by the base pair states (i.e., all the states except the first and last ones in Eq. **S13**) yields a diagonalization matrix **u**. The bloc-diagonalization matrix is then given by:

$$\mathbf{U} = \begin{pmatrix} \mathbb{I} & & \\ & \mathbf{u} & \\ & & \mathbb{I} \end{pmatrix}. \quad \textbf{[S14]}$$

Applying this rotation matrix on the Hamiltonian (Eq. **S13**) (i.e., $\mathcal{H}_{bd} = \mathbf{U}^{\dagger}\mathcal{H}\mathbf{U}$) gives the bloc-diagonal Hamiltonian:

$$\mathcal{H}_{bd} = \begin{pmatrix} E_{S_A} & V_{a1} & \dots & \dots & V_{aN} & 0 \\ V_{a1} & \epsilon_1 & 0 & & & V_{1b} \\ \vdots & 0 & \ddots & \ddots & & \vdots \\ \vdots & & \ddots & \ddots & 0 & \vdots \\ V_{aN} & & & 0 & \epsilon_N & V_{bN} \\ 0 & V_{1b} & \dots & \dots & V_{bN} & E_{S_b} \end{pmatrix}, \quad \textbf{[S15]}$$

where ϵ_k is the energy of the kth DCC and V_{ak} and V_{kb} are the couplings between kth channel and S_a and S_b, respectively. The values of these couplings and energies are reported in Table S5. As seen in this Table S5 and also in Fig. 4, depending on the location of the A:T/G:C substitution along the sequence, different DCCs are affected. The replacement of the first A:T base pair with G:C decreases the energy of the two lowest DCCs, ϕ_1 and ϕ_2. Due to its localization near the hole donor, ϕ_1 interacts very weakly with the hole acceptor and plays a minor role in the charge transfer process. The weak energy reduction of ϕ_2 induced by an A:T/G:C substitution of the first base pair is therefore responsible for the small increase in k_a observed for the GA_n compared with the A_n series. As explained in the main text, an A:T/G:C substitution performed at the end of hairpin leads to an important energy reduction of ϕ_6 that becomes nearly degenerate with ϕ_3 at about 1.40 eV. As a consequence, two strongly DCCs are created and form extremely efficient conduction channels. Due to the weak couplings, V_{xn}, compared with the energies, ϵ_nm, the transfer rate via the nth DCCs can be approximated by:

$$k_n \simeq \frac{2\pi}{\hbar} < \left| \frac{V_{an} V_{nb}}{\epsilon_n} \right| >, \quad \textbf{[S16]}$$

where the symbol $< >$ indicates the average over the dynamical disorder. As an example, the values of k_n reported in Table S5 represent the average over 10,000 realizations of the Hamiltonian. The sum of the k_n for a given sequence gives an approximate value of the arrival rate k_a obtained from the full quantum mechanical calculations. It is obvious from this table that in the case of A_5G, the DCCs ϕ_3 and ϕ_4 are the principal conduction channels.

1. Renaud N, Berlin YA, Lewis FD, Ratner MA (2013) Between superexchange and hopping: An intermediate charge-transfer mechanism in poly(A)-poly(T) DNA hairpins. *J Am Chem Soc* 135(10):3953–3963.
2. Grozema FC, et al. (2008) Effect of structural dynamics on charge transfer in DNA hairpins. *J Am Chem Soc* 130(15):5157–5166.
3. Lewis FD, et al. (2006) Crossover from superexchange to hopping as the mechanism for photoinduced charge transfer in DNA hairpin conjugates. *J Am Chem Soc* 128(3):791–800.
4. Senthilkumar K, Grozema FC, Guerra CF, Bickelhaupt FM, Siebbeles LDA (2003) Mapping the sites for selective oxidation of guanines in DNA. *J Am Chem Soc* 125(45):13658–13659.
5. Mishra D, Pal S (2009) Ionization potential and structure relaxation of adenine, thymine, guanine and cytosine bases and their base pairs: A quantification of reactive sites. *J Mol Struct THEOCHEM* 902(1-3):96–102.
6. Grozema FC, et al. (2009) Effect of GC base pairs on charge transfer through DNA hairpins: The importance of electrostatic interactions. *J Am Chem Soc* 131(40): 14204–14205.
7. Paavola J, Pillo J, Suominen K-A, Maniscalco S (2009) Environment-dependent dissipation in quantum brownian motion. *Phys Rev A* 79(5):05120.
8. Weiss U (1999) *Quantum Dissipative Systems* (World Scientific, Singapore).
9. Taniguchi M, Kawai T (2005) Electron-molecular-vibration coupling for small polarons in DNAs. *Phys Rev E Stat Nonlin Soft Matter Phys* 72(6 Pt 1):061909.
10. Lewis FD, Daublain P, Cohen B, Vura-Weis J, Wasielewski MR (2008) The influence of guanine on DNA hole transport efficiency. *Angew Chem Int Ed Engl* 47(20): 3798–3800.

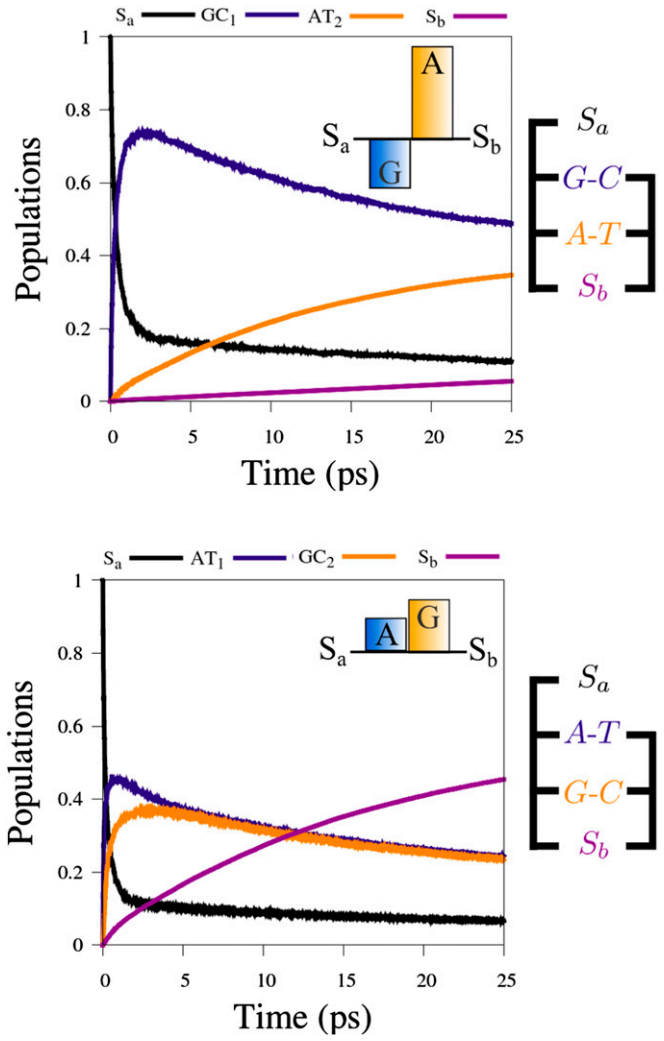

Fig. S1. Evolution of the initial hole density along *GA* (*Upper*) and *AG* (*Lower*). Charge transfer is significantly more efficient along *AG* than along *GA*.

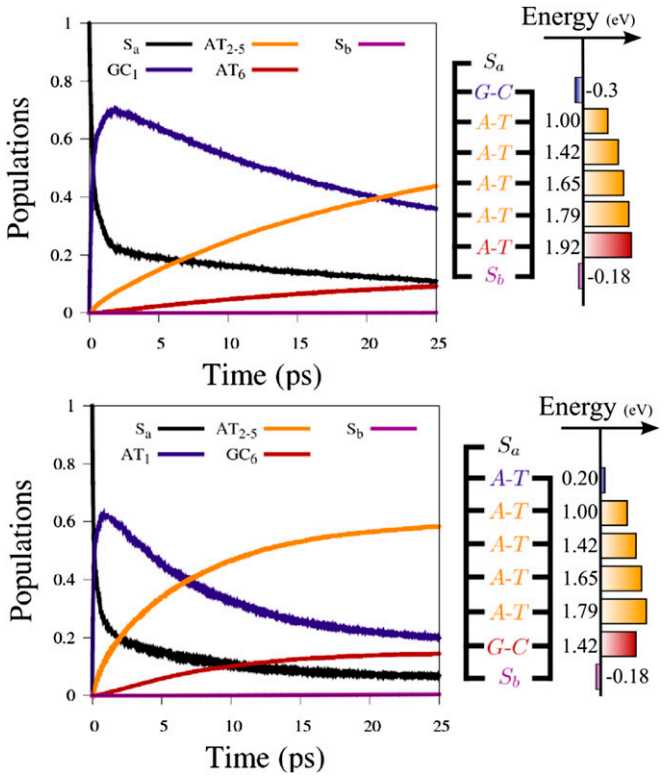

Fig. S2. Time evolution of the hole population of various base pairs in GA_5 (*Upper*) and A_5G (*Lower*) hairpins. Although the population on S_b remains low (0.01) for both systems, numerical data clearly show that charge transfer is faster in the case where the G:C pair is located next to S_b than in the case where this pair is located next to the hole donor S_a.

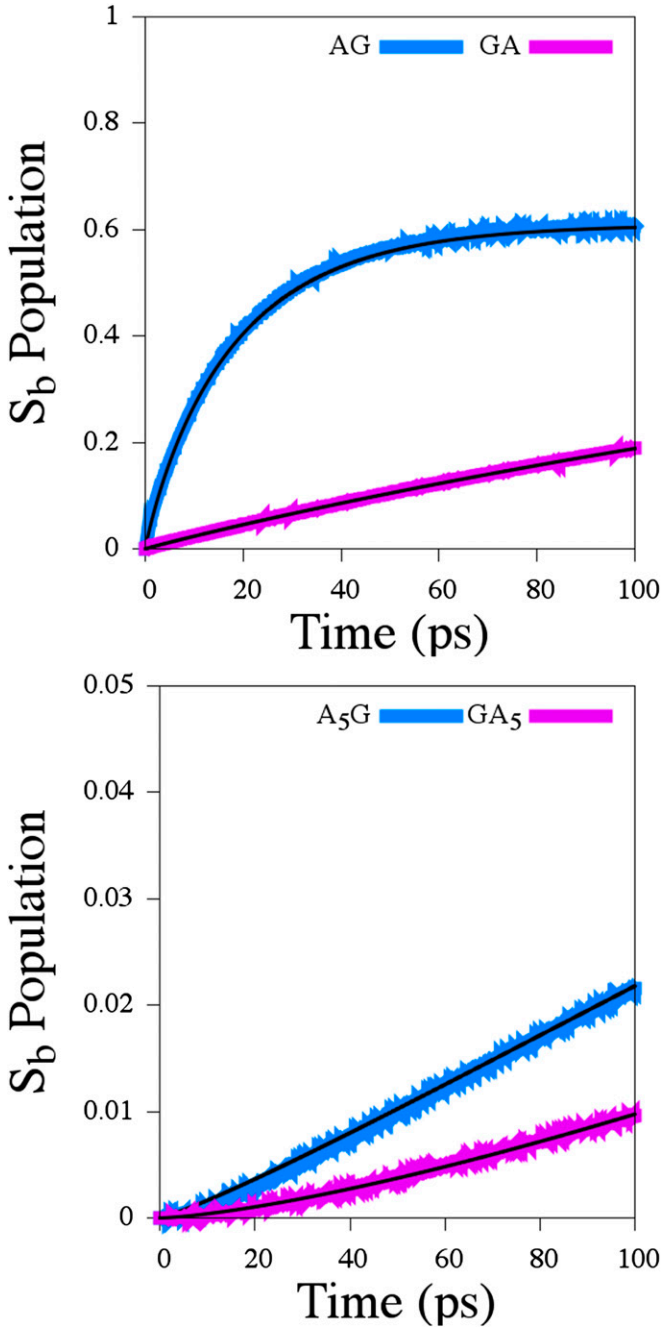

Fig. S3. Fit of the time-dependent evolution of hole density localized on S_b for *AG* and *GA* (*Upper*) and A_5G and GA_5 (*Lower*). Note the deviation from simple exponential for the long hairpins.

Table S1. Theoretical values of the arrival rate (k_a) and the charge separation quantum yield (Φ_a) obtained for all the sequences shown in Fig. 1

Sequence	k_a, ns^{-1}	Φ_a	χ	Sequence	k_a, ns^{-1}	Φ_a	χ	Sequence	k_a, ns^{-1}	Φ_a	χ
A_1	186.20	0.78	0.6								
A_2	10.00	0.45	1.0	GA	11.5	0.27	1.1	AG	54.95	0.61	0.8
A_3	1.69	0.10	1.1	GA_2	2.69	0.18	1.3	A_2G	10.23	0.15	1.3
A_4	1.07	0.09	1.1	GA_3	1.99	0.19	1.3	A_3G	5.49	0.13	1.2
A_5	0.69	0.09	1.2	GA_4	1.14	0.15	1.2	A_4G	3.01	0.14	1.1
A_6	0.54	0.06	1.2	GA_5	0.81	0.18	1.3	A_5G	2.04	0.09	1.1
AGA	4.78	0.12	1.1								
AGA_2	2.08	0.11	1.2	A_2GA	2.29	0.13	1.1				
AGA_3	1.34	0.10	1.2	A_3GA	1.54	0.10	1.2	A_2GA_2	1.81	0.10	1.2
AGA_4	0.93	0.10	1.2	A_4GA	0.97	0.09	1.2	A_3GA_2	0.95	0.09	1.2

Table S2. Scaling factors and falloff parameters for the arrival rate distance dependence given in Eq. S9

Sequence	κ_1, ps^{-1}	β, Å^{-1}	κ_2, ns^{-1}	η
A_n	8.00	0.85	1.60	2.0
GA_n	2.50	0.75	8.00	2.0
AGA_n	1.05	0.55	9.00	1.9
A_nG	3.00	0.55	20.00	2.0

Table S3. Degree of localization of the hole density ($\mathcal{L}$) and participation ratio of the *G* base ($\mathcal{R}_G$) (details are provided in *SI Text*)

Sequence	$\mathcal{L}$	$\Delta\mathcal{L}$	$\mathcal{R}_G$	$\Delta\mathcal{R}_G$
A_6	0.23	—	—	—
GA_5	0.32	+39%	0.51	+55%
AGA_4	0.20	−13%	0.27	+80%
A_2GA_3	0.24	—	0.15	+36%
A_3GA_2	0.23	—	0.11	+23%
A_4GA	0.24	—	0.10	+17%
A_5G	0.23	—	0.09	+11%

Table S4. Transfer rates between neighboring base pairs for different sequences ($k_{i\to j}$) and final transfer rate between the last base pair and the hole acceptor (k_f)

Rate	A_6	G_6	GA_5	AGA_4	A_2GA_3	A_3GA_2	A_4GA	A_5G	Units
$k_{1\to2}$	0.31	0.32	0.06	5.40	0.46	0.38	0.36	0.29	
$k_{2\to3}$	0.29	0.31	0.29	0.09	3.81	0.37	0.26	0.30	
$k_{3\to4}$	1.11	1.10	3.31	0.99	0.08	1.74	1.09	0.99	ps^{-1}
$k_{4\to5}$	2.02	2.83	2.42	3.31	4.45	0.16	1.13	2.59	
$k_{5\to6}$	7.05	25.9	1.31	3.06	2.29	5.08	0.31	1.35	
k_f	0.23	1.96	0.84	0.96	0.99	1.00	0.99	2.10	ns^{-1}

Table S5. Couplings V_{an} and V_{bn} (meV), energies ϵ_n (eV), and transfer rate k_n (ns^{-1}) for each DCC (ϕ_n) of different sequences

	A_6				GA_5				A_2GA_3				A_5G			
ϕ_n	V_{an}	ϵ_n	V_{bn}	k_n	V_{an}	ϵ_n	V_{bn}	k_n	V_{an}	ϵ_n	V_{bn}	k_n	V_{an}	ϵ_n	V_{bn}	k_n
$n = 1$	4.99	0.19	10^{-6}	10^{-4}	4.99	−0.69	10^{-7}	10^{-4}	4.98	0.19	10^{-6}	10^{-3}	4.99	0.19	10^{-5}	10^{-4}
$n = 2$	0.31	0.99	10^{-3}	10^{-3}	0.01	0.99	10^{-3}	0.01	0.17	0.88	10^{-3}	0.02	0.31	0.99	0.01	0.09
$n = 3$	0.02	1.39	0.23	0.05	10^{-3}	1.39	0.23	0.05	0.26	1.02	10^{-3}	0.04	0.02	1.39	8.02	0.47
$n = 4$	10^{-3}	1.64	5.47	0.09	10^{-4}	1.64	5.47	0.10	10^{-5}	1.63	5.10	0.11	10^{-3}	1.42	98.6	0.52
$n = 5$	10^{-4}	1.79	33.7	0.06	10^{-5}	1.79	33.7	0.08	10^{-6}	1.79	33.7	0.13	10^{-3}	1.64	8.56	0.16
$n = 6$	10^{-5}	1.94	93.9	0.01	10^{-6}	1.94	93.9	0.02	10^{-6}	1.94	93.9	0.04	10^{-4}	1.82	11.79	0.02